McGill/94–17.

Momentum–dependent nuclear mean fields and collective flow in heavy ion collisions

Jianming Zhang*, Subal Das Gupta†, and Charles Gale‡
Physics Department, McGill University
3600 University St., Montréal QC, Canada H3A–2T8

Abstract

We use the Boltzmann-Uehling-Uhlenbeck model to simulate the dynamical evolution of heavy ion collisions and to compare the effects of two parametrizations of the momentum–dependent nuclear mean field that have identical properties in cold nuclear matter. We compare with recent data on nuclear flow, as characterized by transverse momentum distributions and flow (F) variables for symmetric and asymmetric systems. We find that the precise functional dependence of the nuclear mean field on the particle momentum is important. With our approach, we also confirm that the difference between symmetric and asymmetric systems can be used to pin down the density and momentum dependence of the nuclear self consistent one–body potential, independently. All the data can be reproduced very well with a momentum–dependent interaction with compressibility K = 210 MeV.

PACS numbers: 25.70;-z, 25.70.Np

*email: jzhang@hep.physics.mcgill.ca

†email: dasgupta@hep.physics.mcgill.ca

‡email: gale@hep.physics.mcgill.ca

I. INTRODUCTION

Over the past decade, the extraction of the nuclear equation of state (EOS) from experimental data has been one of the main goals of intermediate energy heavy ion collisions. The nuclear EOS plays a major role in the physics of colliding nuclei at high energies and also has a major influence in the theory of supernovæ explosions and neutron star properties [1]. Information on the EOS, as characterized by its coefficient of nuclear compressibility, K, can also be deduced from detailed Hartree–Fock plus RPA analysis of giant monopole resonances in finite nuclei [2].

In the framework of heavy ion collision physics in the 100 MeV/A $\sim$ 2 GeV/A energy regime and its relation to the nuclear EOS, the measurement and theoretical interpretation of collective flow observables have been vital [3]. Among the many models suggested to describe theoretically heavy ion collisions at such energies, the Boltzmann-Uehling-Uhlenbeck (BUU) approach model has proven to be very successful [4]. In BUU simulations, nucleons can suffer hard collisions and can also move on curved trajectories, owing to interaction with the self–consistent nuclear mean field. The properties of the mean field are crucial to such calculations and can also be directly related to the nuclear equation of state. Some effort has been devoted to obtain realistic nuclear mean fields that could be used in practice within such numerical approaches.

Early on in microscopic analyses, it appeared that the data on nuclear flow, as characterized by transverse momentum plots [5,6] and flow angle distributions [7] demanded an equation of state with a high compressibility coefficient (K $\approx$ 380 MeV) [8]. However, it was later shown that if a reasonable momentum dependence was introduced in the nuclear mean field, a lower compressibility would be favored in the interpretation of the experimental data [9–11]. In fact, Pan and Danielewicz [12] have recently shown that flow data for asymmetric systems could differentiate between a hard momentum–independent EOS and a soft momentum–dependent EOS, favoring the latter. Finally, it is clear that the momentum dependence of the nuclear mean field is an unavoidable feature for a fundamental understanding of nuclear matter properties [13] and for the successful interpretation of current heavy ion data.

Additional properties of momentum–dependent mean fields have also emerged in the BUU analysis of heavy collisions. Different sets of momentum–dependent parametrizations sharing a common compressibility coefficient have been used. We will concentrate on two of those. We label them GBD [9] and MDYI [14], in accordance with the (quoted) articles in which they have been introduced. This nomenclature has been used previously [11]. Pan and Danielewicz [12] have used a GBD-type parametrization. Another momentum–dependent potential used in one-body numerical simulations is associated with the Gogny interaction [15]. The properties of the GBD and MDYI potentials are somewhat similar in the ground state, but they will have different behaviors in actual dynamical situations [14,16]. We shall discuss this aspect in the present paper.

Stimulated by the findings of Ref. [12], we have analyzed the quantitative differences between GBD and MDYI–type approaches. We also give our own opinion as to which parametrization should be used in calculations where nonequilibrium effects can be important, as in intermediate energy heavy ion collisions. We further explore the impact of our conclusions on the determination of the nuclear EOS, by comparing with current heavy ion

data. We perform BUU calculations for symmetric and asymmetric projectile–target combinations, at various colliding energies. We also comment on the quantitative importance of angular momentum conservation at the microscopic level in the interpretation of nuclear transverse momentum data. Our paper is organized in the following way: in the next section we give a detailed presentation of the nuclear mean fields used in our BUU calculations. The following section analyzes the generation of transverse momentum. We then compare with experimental data and we finally conclude.

II. NUCLEAR MOMENTUM–DEPENDENT MEAN FIELDS

As mentioned above, different forms of phenomenological momentum–dependent potentials are found in BUU applications. Gale, Bertsch and Das Gupta employed a parametrization of the potential energy density that can be written as [9]

$$V_{\rm GBD}\left(\rho(\vec{r})\right) = \frac{A}{2}\frac{\rho^2(\vec{r})}{\rho_0} + \frac{B}{\sigma+1}\frac{\rho^{\sigma+1}(\vec{r})}{\rho_0^{\sigma}} + \frac{C\rho(\vec{r})}{\rho_0}\int d^3p\ \frac{f(\vec{r},\vec{p})}{1+\left[\frac{\vec{p}-<\vec{p}>}{\Lambda}\right]^2} \tag{2.1}$$

The corresponding mean field (GBD) is obtained by taking a functional derivative with respect to the single–particle occupation function; $U = \frac{\delta V}{\delta f}|_{\vec{p}}$. One then obtains

$$U_{\rm GBD}\left(\rho(\vec{r}),\vec{p}\right) = A\left(\frac{\rho(\vec{r})}{\rho_0}\right) + B\left(\frac{\rho(\vec{r})}{\rho_0}\right)^{\sigma} + \frac{C}{\rho_0}\int d^3p'\frac{f(\vec{r},\vec{p}\,')}{1+\left[\frac{\vec{p}\,'-<\vec{p}>}{\Lambda}\right]^2} + \frac{C}{\rho_0}\frac{\rho}{1+\left[\frac{\vec{p}-<\vec{p}>}{\Lambda}\right]^2}\ , \tag{2.2}$$

where $\vec{p}$ is the momentum of the particle, $<\vec{p}>$ is a local momentum average, and $f(\vec{r},\vec{p})$ is the phase space occupation density. This quantity is normalized such that the nuclear density $\rho(\vec{r}) = \int d^3p\ f(\vec{r},\vec{p})$. There are five parameters to be determined in $U_{\rm GBD}(\rho(\vec{r}),\vec{p})$. Previously [9], two of them were chosen arbitrarily: the momentum scale $\Lambda = 400$ MeV and $\sigma = 7/6$. This exponent has an especially large influence on the nuclear equation of state compressibility coefficient, K. We further required the following at the saturation density: (i) the effective mass m^*/m was set to 0.7 at the Fermi surface, and (ii) the total energy per nucleon was adjusted to reproduce the volume term of the semi–empirical mass formula, E/A $= -16$ MeV. We used $\rho_0 = 0.163\ fm^{-3}$ and thus obtained K = 215 MeV.

Some subsequent work by Welke et al. [14] used an improved parametrization

$$V_{\rm MDYI}(\rho(\vec{r}) = \frac{A}{2}\frac{\rho^2(\vec{r})}{\rho_0} + \frac{B}{\sigma+1}\frac{\rho^{\sigma+1}(\vec{r})}{\rho_0^{\sigma}} + \frac{C}{\rho_0}\int\int d^3p\, d^3p'\frac{f(\vec{r},\vec{p})f(\vec{r},\vec{p}\,')}{1+\left[\frac{\vec{p}-\vec{p}\,'}{\Lambda}\right]^2} \tag{2.3}$$

which leads to the other form of the momentum–dependent potential we shall consider:

$$U_{\rm MDYI}(\rho(\vec{r}),\vec{p}) = A\left(\frac{\rho(\vec{r})}{\rho_0}\right) + B\left(\frac{\rho(\vec{r})}{\rho_0}\right)^{\sigma} + 2\ \frac{C}{\rho_0}\int d^3p'\frac{f(\vec{r},\vec{p}\,')}{1+\left[\frac{\vec{p}-\vec{p}\,'}{\Lambda}\right]^2}\ . \tag{2.4}$$

The five constants A, B, C, σ, and Λ in $U_{\rm MDYI}(\rho(\vec{r}),\vec{p})$ were set by demanding that, at saturation: E/A $= -16$ MeV, K = 215 MeV, the real part of the optical potential

$U(\rho_0,\ p\ =\ 0)\ =\ -75$ MeV and $U(\rho_0,\ \frac{p^2}{2m}\ =\ 300\ \text{MeV})\ =\ 0$. It then follows that $U(\rho_0,\ p\ \rightarrow\ \infty)\ =\ 30.5$ MeV and that the effective mass $m^*/m = 0.67$, at the Fermi surface. The agreement of $U_{\rm MDYI}$ with the real part of the optical potential as extracted from experiment is remarkable, at both low and high energies [17]. To clarify the origins of these parametrizations, we state here that a Yukawa interaction would have a mean field whose exchange term would be a momentum–dependent expression of the MDYI type [14]. The GBD potential energy density can be obtained from its MDYI countrepart by replacing $\vec{p}'$ in the denominator of the integrand of Eq. (2.3) by its average, $<\vec{p}'>$. The momentum–dependent term of the MDYI mean field is attractive and important at low momentum, but it weakens and disappears at very high momentum. Even though both of the above parametrizations (GBD and MDYI) can share the same compressibility K, the quantities $U(\rho_0,\ p\rightarrow\ \infty)$ and the effective mass m* can be different. The value of $U(\rho_0,\ p\rightarrow\ \infty)$ has important consequences for the modelling of nuclear collisions at high energies, as we shall see.

In this work, for the sake of consistence and for the purpose of a quantitative comparison with Ref. [12], we reset the five constants in our GBD and our MDYI potentials. For both parametrizations we require that $\sigma\ =\ 12/11$, E/A $= -16$ MeV, $\rho_0\ =\ 0.15\ fm^{-3}$, $U(\rho, p\rightarrow\infty)\ =\ 30.5$ MeV, and $m^*/m = 0.67$. We then obtain K = 210 MeV, for both potentials. We call these the new MDYI (NMDYI) and new GBD (NGBD), respectively, to distinguish these new parameter sets from the previous ones. We further note that both NGBD and NMDYI give a similar excellent fit of the high energy optical potential (defined at saturation density), a desirable and important feature.

If one neglects the momentum–dependent term, which means C=0, the mean field is a function of the nuclear density ρ alone. This simple Skyrme parametrization has the form (making the $\vec{r}$ dependence implicit):

$$U(\rho) = A\ (\frac{\rho}{\rho_0}) + B\ (\frac{\rho}{\rho_0})^\sigma\ . \tag{2.5}$$

We may thus further define two additional parameter sets. The first is a Hard potential (K = 373 MeV) and the second a Soft potential (K = 200 MeV). The parameters for the GBD, MDYI, NGBD, NMDYI, and momentum–independent Hard and Soft potentials are summarized in Table 1, together with a hard MDYI potential(HM), which has K = 373 MeV. Note that for all those potentials $P(\rho_0, T=0) = 0$ and $E/A(\rho_0, T=0)\ =\ -16$ MeV.

Fig. 1 shows the difference between the NGBD and NMDYI single–particle potentials. Both those potentials produce the same bulk nuclear matter properties at equilibrium. We plot the potentials as a function of wave vector k, for densities ranging from 0.1 to 0.5 fm^{-3}, in units of 0.1 fm^{-3}. Both potentials have a somewhat similar momentum dependence, but for higher densities the NGBD is more attractive at values of $k \lesssim k_{\rm F}$ and notably more repulsive at $k \gtrsim k_{\rm F}$. This behaviour has been noted previously [14]. We thus insist on the following important fact: even though the two interactions have an identical high–momentum behaviour for $\rho = \rho_0$, the similarity in their asymptotic values is not guaranteed for densities other than equilibrium nuclear matter density. The influence on the collective observables will be discussed in the following sections. As an additional comparison, we also show the momentum dependence of the GBD and NGBD parametrizations in Fig. 2. The two parametrizations yield almost identical compressibilities (c.f. Table 1), but the high

momentum NGBD is much more repulsive owing mainly to its asymptotic optical potential: $U(\rho, p \rightarrow \infty)$. Also comparing to Wiringa's microscopic calculations [18] one realizes that NMDYI is very close in behaviour to that of the UV14 + UVII interaction, over a wide range of momenta and densities. On the other hand, the high momentum part of NGBD reaches values closer to that of the UV14 + TNI potential. In addition to fitting nuclear matter properties, the potentials described by Wiringa can reproduce nucleon-nucleon scattering and few–body data.

III. TRANSVERSE MOMENTUM

One important technique proposed to quantify the flow of nuclear matter is the transverse momentum analysis [5]. This method has also been used to clarify the transverse momentum generating features of different nuclear mean fields in the BUU approach to nucleus–nucleus dynamics. In the framework of such studies it has been shown that under certain circumstances, a soft momentum–dependent potential can produce about the same transverse momentum as that of a hard momentum independent–interaction [9,10]. An effort to understand this was made in reference [11]. In order to further highlight the behaviour in a dynamical situation of the Hard, GBD, NGBD and NMDYI potentials, we plot in Fig. 3 the time evolution of the average transverse momentum for a symmetric Nb + Nb collision at projectile kinetic energy E = 400 MeV/nucleon at an impact parameter b = 2.1 fm. A sizeable difference in the saturated transverse momentum is observed. The hard momentum–independent potential follows the behavior of the soft momentum–dependent one quite closely, at this impact parameter. The asymptotic values of their average transverse momentum are only 4 MeV/c apart. We comment on the behaviour of the momentum–dependent interactions below.

By turning off the hard nucleon-nucleon collisions, one can study the Vlasov behaviour of the Hard, GBD NGBD and NMDYI potentials. From Fig. 4 one realizes that the momentum–dependent single particle potentials alone can generate large transverse momenta, whereas the Hard potential can only yield very small transverse momenta. These results are similar to the results of Ref. [11]. Comparing Figs. 3 and 4, we can further deduce another important fact: the role of hard two-body collisions is quite different, depending on whether the nuclear mean field is momentum–dependent or not. Comparing the Hard and NMDYI potentials, the fraction of the net average transverse momentum generated by adding the collision term to the Vlasov equation is $\approx$ 100 % and $\approx$ 42 %, respectively. However, it is important to point out that the transverse momentum is generated by the nuclear mean field and the hard two–body collisions in a highly non–linear fashion. Fig. 4 also tells us that, even though the GBD and NGBD potentials have the same functional dependence on momentum and almost identical compressibilities, they produce net transverse momenta that are very different from each other. As discussed in section II, this result can be understood simply in terms of the different asymptotic values of the respective one–body potentials. Continuing our interpretation of the results in Fig. 4, we find the following interesting fact: the NGBD and NMDYI potentials produce average transverse momenta in the Vlasov mode that differ by $\approx$ 10 MeV/c. Both these parametrizations share the same $U(\rho_0, \infty)$ and K. As mentioned previously, fitting the static nuclear matter properties and

optical potential is not enough to predict unambiguously the consequences of the different interactions in nonequilibrium situations. It is also likely that realistic cases will also carry the added complication that generally, $<\vec{p}> \neq 0$ in the GBD formulation of the one–body potential.

Fig. 5 shows the average in–plane transverse momentum, calculated in the BUU model, as a function of centre of mass rapidity. From this figure, it is also clear that NGBD is more repulsive than NMDYI [14]. We will discuss later which interaction we favor, from a theoretical point of view.

IV. COMPARISON WITH DATA

In this section, we compare BUU calculations with experimental data. We will first concentrate on values of the flow parameter F and transverse momentum distributions, as measured in asymmetric heavy ion reactions by the DIOGENE collaboration [19] and by the Riverside/GSI/LBL Streamer chamber group [20]. The flow parameter F is defined as

$$F = \left[\frac{d < P_x/m >}{dy}\right]_{y=y_0} . \tag{4.1}$$

Here $< P_x >$ is the average value of the transverse momentum projection on the reaction plane and y_0 is the rapidity at the intercept: $< P_x >|_{y_0} = 0$. Since the experimental efficiency cuts influence the observables, corresponding restrictions have to be applied to the theoretical calculations in order to compare with measured values.

Following Ref. 12, we first turn to measurements by the DIOGENE collaboration. There, the laboratory polar angle of the particles is limited by

$$20^\circ \leq \theta \leq 132^\circ . \tag{4.2}$$

The transverse momentum $P_\perp$ of the particles have to satisfy

$$P_\perp/m > 0.36 + 0.72y \qquad \text{if } y < 0 \tag{4.3}$$

$$P_\perp/m \geq 0.36 - 0.8y \qquad \text{if } y \geq 0 . \tag{4.4}$$

The measurements of rapidity distribution for "pseudo–protons", around y_0 are plotted in Fig.6 (a) for Ar + Pb at 400MeV/nucleon at an impact parameter b=4.5 fm. Well-known geometrical arguments are used to estimate the impact parameter [22]. The data shows a linear rapidity dependence of $< P_x >$, in the interval [0, 1]. The flow parameter F is obtained by fitting the data to a straight line in the appropriate interval, as shown on Fig. 6. The BUU calculations were performed with 120 parallel simulations to minimize numerical fluctuations, and with free space nucleon-nucleon scattering cross sections. We note in passing that since the two-body collisions contribute more to the transverse flow with a momentum–independent potential than with a momentum–dependent potential as discussed previously, this observable is not expected to be greatly sensitive to reasonable

variations in the in–medium cross sections. To illustrate this point, compare also Fig. 3 with Fig. 4.

Our simulation results also show that the transverse momentum $< P_x >$depends linearly on the rapidity around $< P_x >=0$ with both NGBD and NMDYI potentials. Fig.6 clearly shows this. The fit to the experimental data is quite good with both interactions. To increase data sensitivity to the model parameters, the extracted values of the flow parameter, F, are plotted as a function of the impact parameters b in Fig.7, together with the relevant data. We see that the overall agreement is quite remarkable with the NMDYI potential whereas the NGBD potential gives a larger values than the experimental measurements. The momentum–independent potential fails completely to reproduce the data. Our calculation results are consistent with the results of Ref. [12], where the data is fitted by a low compressibility GBD–type potential. We also confirm the important finding that the asymmetric system can nicely separate out interactions of a similar compressibility but with a different momentum dependence. The results associated with the hard and soft interactions of the MDYI type do not differ much in this plot.

Now we turn to rapidity distributions as measured by the Streamer Chamber. The results of the analysis are presented in terms of the mean in plane transverse momentum as a function of normalized rapidity in Ar + Pb central collisions at 400 and 800 MeV/nucleon, respectively. All protons, whether free or bound in clusters, have been included. Fig. 8 shows the calculation results of rapidity distributions with the NMDYI and NGBD potentials at 400MeV/A in comparison with the data. The behaviour differs slightly from the common S shape [6] due to the asymmetry in collision geometry. It also differs from the linear DIOGENE data as the two detectors have widely different acceptances. In the calculation, the maximum impact parameter was evaluated within a geometrical clean cut model. The value of b_{max} used was 5.8 fm. Our calculations with the NMDYI potential reproduce the data very well. A considerably larger transverse momentum transfer was generated by the NGBD potential simulations. In Fig. 9 we compare the results obtained with the two potentials with data obtained with the same projectile–target combination, at 800 MeV/A. We reach similar conclusions as in the 400 MeV/A case.

Fig.10 presents the excitation function of the average in–plane transverse momentum in Ar + Pb collisions. The average transverse momentum per nucleon is evaluated from protons with rapidities in the c.m. system greater than 0.1, 0.15, 0.2 and 0.3 for beam energies 400, 800, 1200 and 1800 MeV/A, respectively. The average BUU transverse momentum with the NGBD and hard MDYI(HM) potentials are much larger than the data. The only good fit is provided by the NMDYI potential. There, the agreement is striking at all energies. Again, a hard momentum–independent potential is completely ruled out by this data.

Summarizing this section so far, we reproduce both the DIOGENE and the Streamer Chamber measurements quite well in terms of BUU microscopic simulations with the MDYI–type momentum–dependent potential, with a compressibility K = 210 MeV. A GBD–type momentum–dependent potential with the same K value is not so successful and a momentum–independent interaction fails completely. Our findings support those of Ref 12: the flow parameter data for asymmetric systems is quite efficient in separating interactions that are momentum–dependent from those that are momentum–independent, even though their compressibility coefficient are the same.

We now turn to a set of preliminary data on symmetric systems [21], as measured by the

EOS TPC Collaboration. Such data are of high quality, virtually free of experimental biases. The EOS Time Projection Chamber, with its simple and seamless acceptance, good particle identification and high statistics, was designed to overcome the limitations of the previous generation of 4π detectors. The Plastic Ball detector, even though having provided a seminal contribution to the field, had a complex acceptance that was not so easily simulated. The Streamer Chamber was somewhat limited by its particle identification capabilities. In the EOS TPC measurements we shall consider, all nuclear fragments species up to ^{4}He are included. The multiplicity trigger was set in order to select an interval centered about the value where the flow has its maximum. This multiplicity interval corresponds to baryon multiplicities $0.6M^{\rm max} \leq M \leq 0.9M^{\rm max}$. $M^{\rm max}$ is a value near the upper limit of the multiplicity spectrum where the height of the distribution has fallen to half its plateau value. In our BUU calculations, we have adjusted our impact parameter limits to reproduce the multiplicity cuts, in a geometrical clean–cut model. The integration was then carried out by sampling several impact parameter values between those two limits. The data are in–plane transverse momentum measurements as a function of rapidity. The flow parameter F could then be evaluated. Fig. 11 shows the TPC data, together with our calculated results. Measurements were made for Au + Au at beam energies 250, 400, 600, 800 and 1200 MeV/A. We display results of calculations with a soft and a stiff momentum–dependent potential. Calculations done with the NMDYI interaction reproduce the data exactly.

Au + Au is a reasonably large system and it might be that there exists effects that could safely be neglected for smaller nuclei at lower energies that are important here. It was brought up recently that an improvement in the angular momentum conservation in the microscopic models could perhaps lead to a re-evaluation of the role played by the nuclear mean field in generating transverse momentum in heavy ion collisions [23]. The quantitative importance of conservation laws in microscopic models of heavy ion collisions has been investigated before [24,25]. In the case at hand, the only difference might come from the fact that we are dealing here with very heavy systems at high energies. Thus the respective role played by two–body scattering and mean field effects might be modified. We have considered two numerical algorithms. In the first approach, whenever two–body scattering occurred at the microscopic level we made sure that the direction of the reaction plane was unchanged in the centre of mass of the colliding nucleons. The other algorithm made sure that angular momentum was conserved *exactly*. Fig. 12(a) displays the effects of reaction plane conservation on the results of BUU calculations, for Au + Au collisions at 1 GeV/A. The impact parameter range and kinematical cuts were adjusted to match those of the TPC. Fig. 12(b) shows the consequences of reaction plane and exact angular momentum conservation on cascade simulations of the same nuclear reaction. The exact algorithms used are described in Ref. 24. The imposition of exact angular momentum conservation increases the flow parameter by roughly 23% in cascade simulations. We can also see that the dominant effect in angular momentum conservation comes from keeping the direction of the reaction plane constant in individual two–body collisions. In the BUU calculations, reaction plane constraints raise the flow by only 8%. The net effect on the transverse momentum can readily by appreciated in those two figures. Basically, the effect on BUU calculations in considerably smaller than in cascade approaches.

V. SUMMARY

We have used the Boltzmann-Uehling-Uhlenbeck equation to describe the dynamics of nucleus-nucleus collisions. Concentrating on the momentum–dependent features of the one–body self–consistent nuclear mean field, we have seen that the precise functional dependence on momentum of the interaction was important. Taking two potentials with the exact same characteristics at saturation density and zero temperature (NGBD and NMDYI), we have shown that their behaviour in situations removed from equilibrium could be quite different. From a purely theoretical point of view we believe that approaches based on MDYI–type interactions are on a firmer basis. In GBD–like approaches, the quantity $< \vec{p} >$ was put in by hand to enforce the Galilean invariance of the potential. MDYI has Galilean invariance from the start and furthermore, the fact that it can be identified with the Fourier transform of a Yukawa potential is pleasing. Both interactions have the virtue of being relatively simple to handle (MDYI is however trickier to implement numerically). Again, in equilibrium or close to equilibrium situations it should make little difference which is used. As far as the results outlined in this paragraph go, our investigations follow in the steps of some of our previous works [11].

Furthermore, keeping in mind the quantitatively different results obtained with NGBD and NMDYI, we have confirmed the idea put forward by Pan and Danielewicz [12]. By performing calculations to address data on symmetric and asymmetric systems at high energies, one can indeed assess the importance of the density–dependent and momentum–dependent terms in the nuclear equation of state, separately. In pursuing this point, we have for the first time compared DIOGENE and EOS TPC data with BUU results. We find that all the data we have considered in this paper can be reproduced with a momentum–dependent interaction with a nuclear compressiblity coefficient of K = 210 MeV. Also, we have verified again the importance of angular momentum conservation on the generation of transverse momentum in high energy heavy ion collisions. Relaxing the conservation law leads to a slight variation in the flow parameter in BUU collisions. This change should be considered in high precision fits of the experimental data as it should undoubtedly lead to lower values of χ^2 [26]. This does not however alter the general conclusions reached in this work.

Finally, it is worth pointing out that after more than a decade of careful experimental investigations and theoretical progress, a consistent picture of the behaviour of nuclear matter at high temperatures and densitites is emerging. Perhaps the crudest way of characterizing the nuclear equation of state is by its compressibilty coefficient and this value is now stabilizing to some number around 210 MeV. The fact that low and high energy heavy ion experiments seem to require compatible values of K is satisfying. The fact that high quality, bias–free, exclusive experimental is now available and will continue to be generated in the immediate future will set even more stringent tests for the models. Some challenging problems remain to be successfully tackled in theory. For example, the area of composite production is an active area of research [27]. In the context of nuclear flow, this is a pressing issue as it now clear that composites bear the greatest sensitivity to collective behaviour in high energy heavy ion collisions.

ACKNOWLEDGMENTS

We wish to acknowledge fruitful discussions with P. Danielewicz, D. Keane and Q. Pan. Our research is supported in part by the Natural Sciences and Engineering Research Council of Canada and in part by the FCAR fund of the Québec government.

REFERENCES

[1] See, for example, Proceedings of the NATO ASI on the Nuclear Equation of State, Peñiscola, Spain 1989, W. Greiner and H. Stöcker ed., NATO ASI Series B: Physics Vols. 216A and 216B, and references therein.

[2] J.P. Blaizot, D. Gogny and B. Grammaticos, Nucl. Phys. **A265**, 315 (1976).

[3] For a review, see H.H. Gutbrod, A.M. Poskanzer, and H.G. Ritter, Rep. Prog. Phys. **52**, 1267(1989); K.H. Kampert, Ann. Rev. Nucl. Part. Phys. **15** , 691 (1989).

[4] G.F. Bertsch and S. Das Gupta, Phys. Rep. **160**, 189 (1988).

[5] P. Danielewicz and G. Odyniec, Phys. Lett. **B 157**, 146 (1985) .

[6] K.G.R. Doss et al., Phys.Rev. Lett. **57**, 302 (1986) .

[7] H.A. Gustafsson et al., Phys. Rev. Lett. **52**, 1590 (1984).

[8] H. Stöcker and W. Greiner, Phys. Rep. **137**, 277 (1986), and references therein.

[9] C. Gale, G. Bertsch and S. Das Gupta, Phys. Rev. **C 35**, 1666 (1987) .

[10] J. Aichelin, A. Rosenhauer, G. Peilert, H. Stoc̈ker and W. Greiner, Phys. Rev. Lett. **58**, 1926 (1987) .

[11] C. Gale, G.M. Welke, M. Prakash, S.J. Lee and S. Das Gupta, Phys. Rev. **C 41**, 1545 (1990) .

[12] Q. Pan and P. Danielewicz, Phys. Rev. Lett. **70**, 2062 (1993); Phys. Rev. Lett. **70**, 3523 (1993).

[13] J.P. Jeukenne, A. Lejeune, and C. Mahaux, Phys. Rep. **25**, 83 (1976).

[14] G.M. Welke, M.Prakash, T.T.S. Kuo, S. Das Gupta and C. Gale, Phys. Rev. **C 38**, 2101 (1988) .

[15] V. de la Mota, F. Sébille, B. Remaud and P. Schuck, Phys. Rev. C **46**, 667 (1992).

[16] V. Koch, Proceedings of the NATO ASI on Nuclear Matter and Heavy Ion Collisions, Les Houches 1989, M. Soyeur, H. Flocard, B. Tamain, and M. Portneuf ed., NATO ASI Series B: Physics Vols. 205B.

[17] L. P. Csernai, G. Fai, C. Gale, and E. Osnes, Phys. Rev. C **46**, 736 (1992).

[18] R.B. Wiringa, Phys. Rev. **C 38**, 2967 (1988) .

[19] M. Demoulins, Ph.D. Thesis, University Paris Sud, 1989 (unpublished);J. Gosset et al., in The Nuclear Equation of State, edited by W. Greiner and H. Stöcker, NATO ASI Series (Plenum, N.Y., 1989) Vol. 216A;M. Demoulins et al., Phys. lett. **B 241**, 479 (1990) .

[20] D. Beavis et al., Phys. Rev. **C 45**, 299 (1992) .

[21] D. Keane *et al.*, Proceedings of the NATO ASI on Hot and Dense Nuclear Matter, Bodrum, Turkey, W. Greiner and H. Stöcker, eds., (Plenum, NY) 1994.

[22] H. Ströbele *et al.*, Phys. Rev. Lett. **49**, 1236(1982);J. J. Molitoris, H. Stöcker, and B. L. Winer, Phys. Rev. C **36**, 220(1987);D. Keane *al.*, *ibid.* **37**, 1447(1988);C. Cavata *et al.*, *ibid.* **42**, 1760(1990).

[23] David E. Kahana, Declan Keane, Yang Pang, Tom Schlagel, and Shan Wang, Kent State University preprint 1994.

[24] C. Gale and S. Das Gupta, Phys. Rev. C **42**, 1577 (1990).

[25] T. J. Shlagel and V. R. Pandharipande, Phys Rev. C **44**, 1601 (1991).

[26] T. J. Schlagel, PhD thesis, University of Illinois at Urbana–Champaign, 1990 (unpublished).

[27] P. Danielewicz and G. F. Bertsch, Nucl. Phys. **A533**, 712 (1991).

TABLES

TABLE I. We write here the parameters and characteristics of the single–particle potentials we have introduced in the main text.

Model	A (MeV)	B (MeV)	σ	C (MeV)	Λ (MeV)	$m*/m$	$U(\rho_0, p_{\rm F})$ (MeV)	$U(\rho_0, 0)$ (MeV)	$U(\rho_0, \infty)$ (MeV)	K (MeV)
Soft	-351.3	300	7/6	0		1	-51.3	-51.3	-51.3	200
Hard	-120.5	69.2	2	0		1	-51.3	-51.3	-51.3	373
GBD	-144.9	203.3	7/6	-75	400	0.7	-53.3	-76.3	-1.34	215
MDYI	-110.44	140.9	1.24	-64.95	415.7	0.67	-52.9	-75	30.5	215
NGBD	-227.5	347.7	12/11	-103.9	495.4	0.67	-51.4	-73.5	30.5	210
NMDYI	-322	352.5	12/11	-62.75	417	0.67	-51.4	-72.4	30.5	210
HM	-9.0	39.5	2.27	-62.75	417	0.67	-51.4	-72.4	30.5	373

FIGURES

FIG. 1. A comparison of the momentum–dependent NMDYI and NGBD potentials, adjusted to produce identical bulk properties in cold nuclear matter. The abscissa shows the wave number. Starting from the bottom, the different curves are for densities of 0.1, 0.2, 0.3, 0.4 and 0.5 fm^{-3}.

FIG. 2. Same caption as in Fig. 1, but with the GBD and NGBD potentials.

FIG. 3. Average in plane transverse momentum per nucleon versus time for BUU calculations of Nb + Nb collisions at 400 MeV/nucleon, at an impact parameter b = 2.1 fm. The results are for the Hard, GBD, NGBD and NMDYI potentials.

FIG. 4. Average in plane transverse momentum per nucleon versus time for Vlasov calculations of Nb + Nb at 400 MeV/nucleon, at an impact parameter b = 2.1 fm. The results are for the Hard, GBD, NGBD and NMDYI potentials.

FIG. 5. Average in plane transverse momentum distributions versus centre of mass rapidity for Nb + Nb for b = 2.1 fm and beam energy 400 MeV/nucleon. The results are for the NGBD and NMDYI interactions.

FIG. 6. Average in plane transverse momentum (divided by the proton mass) as a function of rapidity in the Ar + Pb reactions at 400 MeV per projectile nucleon at an impact parameter b=4.5 fm. The solid and dashed lines represent linear fits through data [19] and calculation, respectively.

FIG. 7. Impact parameter dependence of the flow parameter F for Ar+Pb reactions. The results of BUU calculations with different single particle potentials, Hard, NGBD, NMDYI and HM, are compared with the data of Ref. [19]. Error bars in the theory reflect statistical errors and are only given for one set of calculations.

FIG. 8. Average in plane transverse momentum as a function of normalized rapidity in central Ar + Pb collisions at 400 MeV per projectile nucleon. The data of Ref. [20] are compared with BUU calculations with the NMDYI and NGBD potentials. Errors bars in the theory reflect statistical errors only and are given for one set of calculations.

FIG. 9. Same caption as in Fig. 8 but with incident kinetic energy 800 MeV/A.

FIG. 10. We plot the excitation function of the average transverse momentum per nucleon in the reaction plane for the forward centre of mass hemisphere as a function of beam energy for Ar+Pb reactions. The data of Ref. [20] are compared with the BUU calculations with the Hard, HM, NGBD and NMDYI potentials. Errors bars in the theory reflect statistical errors only and are given for one set of calculations.

FIG. 11. We plot the excitation function of the flow parameter $F' = F \times y^{\rm cm}_{\rm beam}$, where F is defined in the main text. The solid squares refer to Au + Au data as measured by the EOS TPC Collaboration [21], the circles are calculations done within the BUU approach, with a soft and stiff compressibility coefficient. The numerical uncertainties in the calculations are of the order of 10%, as previously.

FIG. 12. We plot the transverse momentum generated in Au + Au collisions at 1 Gev/A against rapidity in the centre of mass. We investigate the consequences of (a) imposing a reaction plane (RP) on each two–body collision in the BUU model and (b) reaction plane (RP) and exact angular momentum conservation (AMC) in a cascade approach.

This figure "fig1-1.png" is available in "png" format from:

http://arXiv.org/ps/nucl-th/9405006v1

This figure "fig2-1.png" is available in "png" format from:

http://arXiv.org/ps/nucl-th/9405006v1

This figure "fig3-1.png" is available in "png" format from:

http://arXiv.org/ps/nucl-th/9405006v1

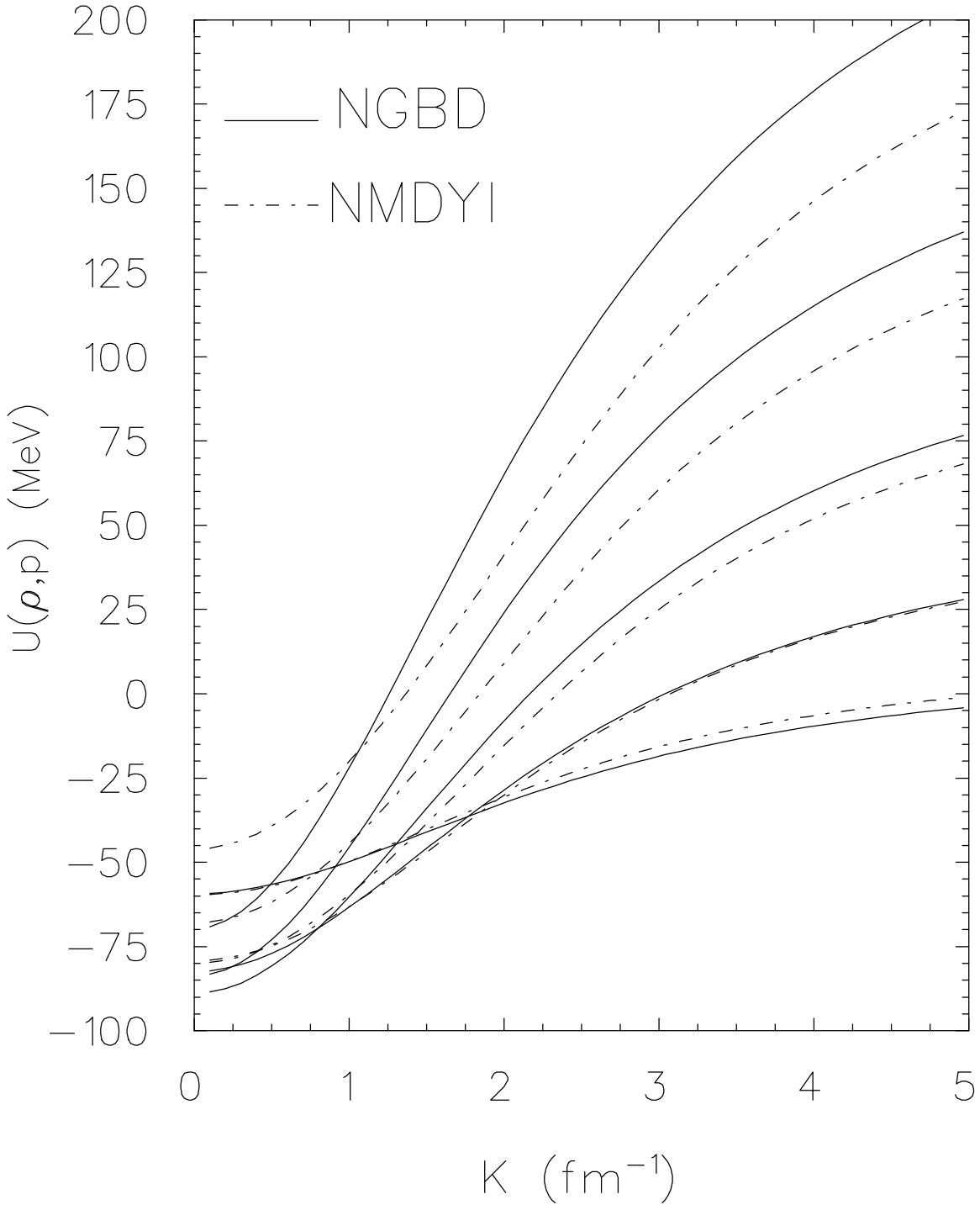
200
175
150
125
100
75
50
25
0
−25
−50
−75
−100
NGBD
NMDYI
U(ρ,p) (MeV)
0
1
2
3
4
5
K (fm⁻¹)

Fig. 1

This figure "fig1-2.png" is available in "png" format from:

http://arXiv.org/ps/nucl-th/9405006v1

This figure "fig2-2.png" is available in "png" format from:

http://arXiv.org/ps/nucl-th/9405006v1

This figure "fig3-2.png" is available in "png" format from:

http://arXiv.org/ps/nucl-th/9405006v1

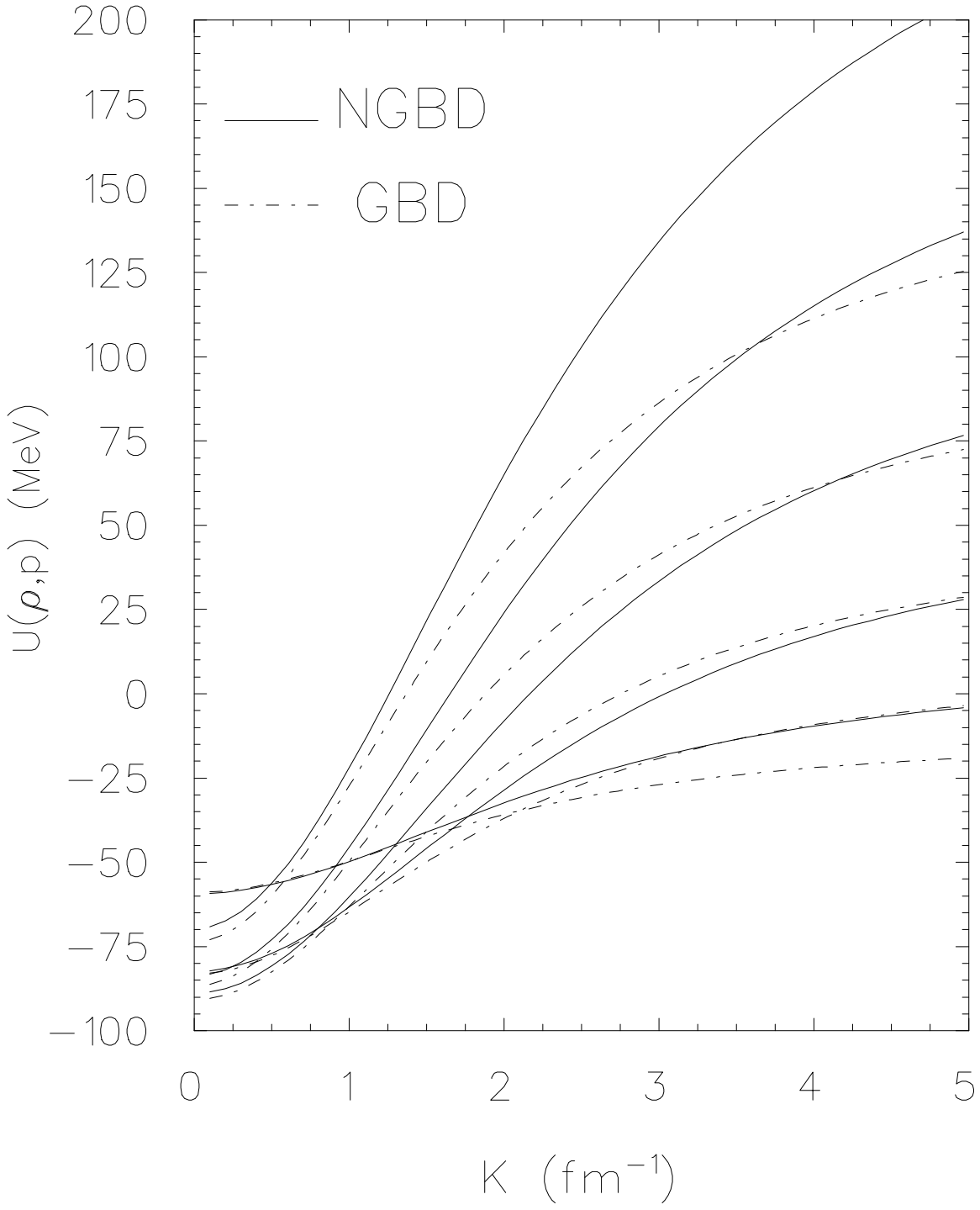
200
175
150
125
100
75
50
25
0
−25
−50
−75
−100
NGBD
GBD
U(ρ,p) (MeV)
0
1
2
3
4
5
K (fm⁻¹)

Fig. 2

This figure "fig1-3.png" is available in "png" format from:

http://arXiv.org/ps/nucl-th/9405006v1

This figure "fig2-3.png" is available in "png" format from:

http://arXiv.org/ps/nucl-th/9405006v1

This figure "fig3-3.png" is available in "png" format from:

http://arXiv.org/ps/nucl-th/9405006v1

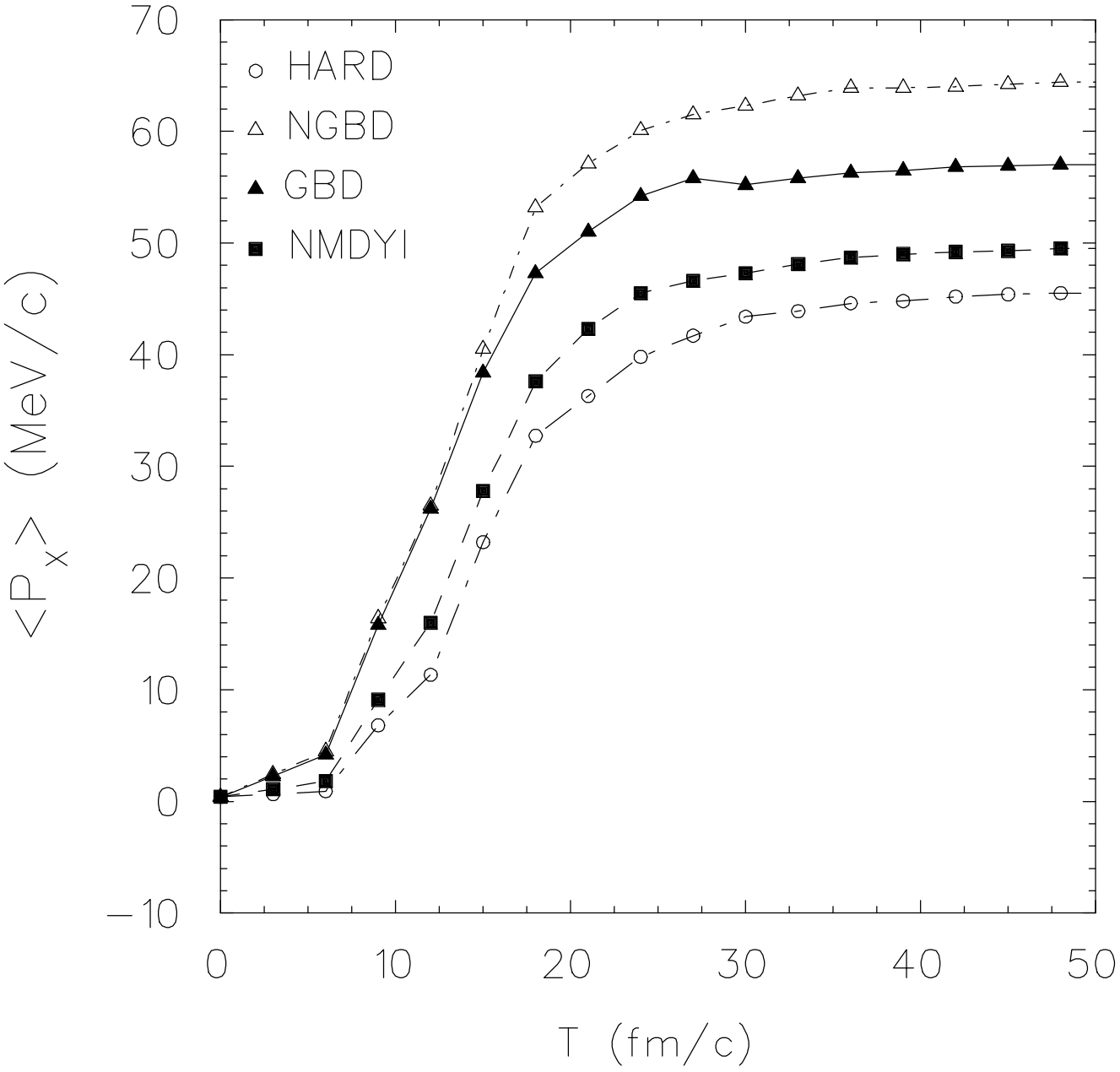
HARD
NGBD
GBD
NMDYI
70
60
50
40
30
20
10
0
−10
0
10
20
30
40
50
<P_x> (MeV/c)
T (fm/c)

Fig. 3

This figure "fig1-4.png" is available in "png" format from:

http://arXiv.org/ps/nucl-th/9405006v1

This figure "fig2-4.png" is available in "png" format from:

http://arXiv.org/ps/nucl-th/9405006v1

This figure "fig3-4.png" is available in "png" format from:

http://arXiv.org/ps/nucl-th/9405006v1

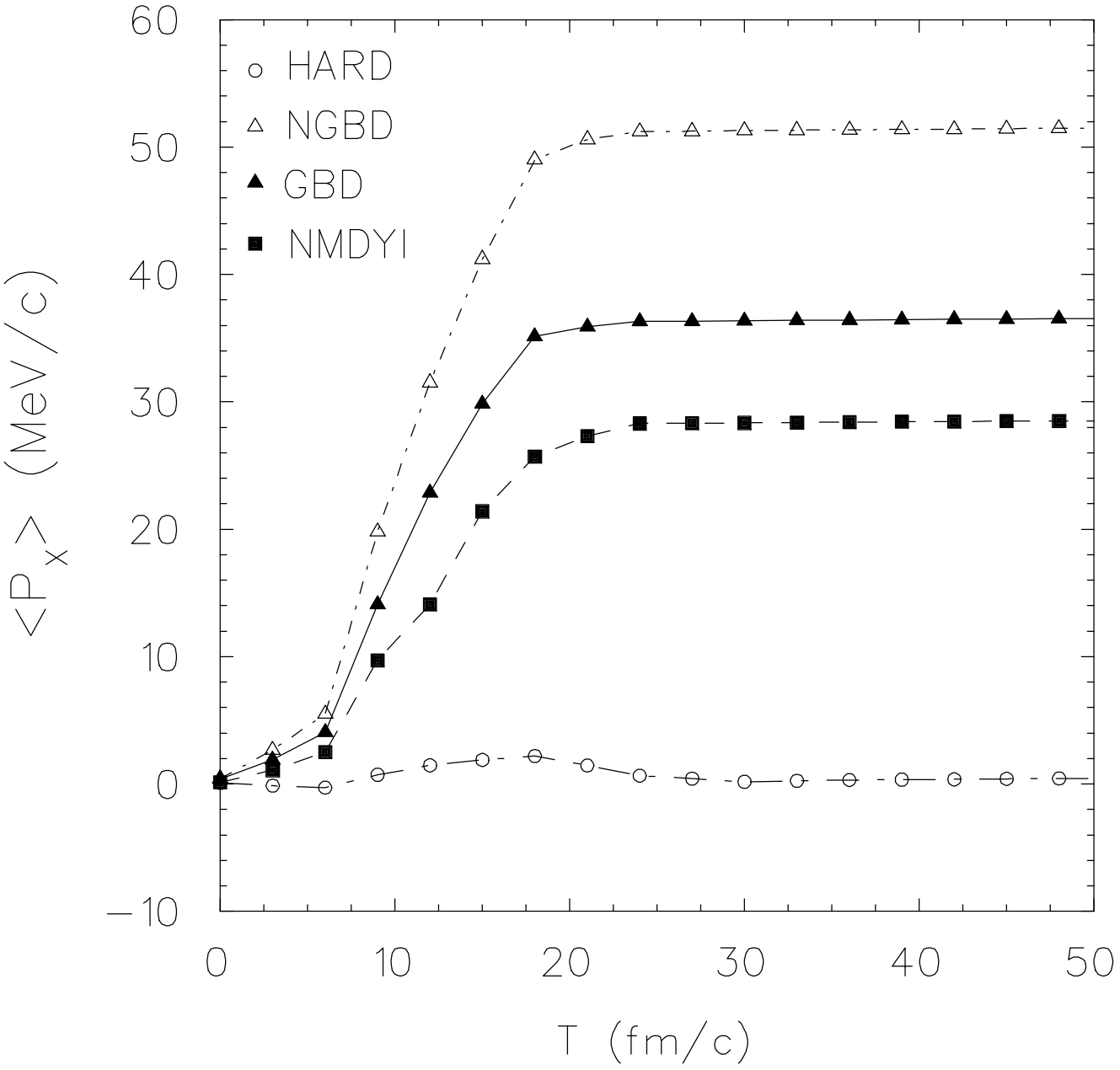
HARD
NGBD
GBD
NMDYI
60
50
40
30
20
10
0
−10
0
10
20
30
40
50
<P_x> (MeV/c)
T (fm/c)

Fig. 4

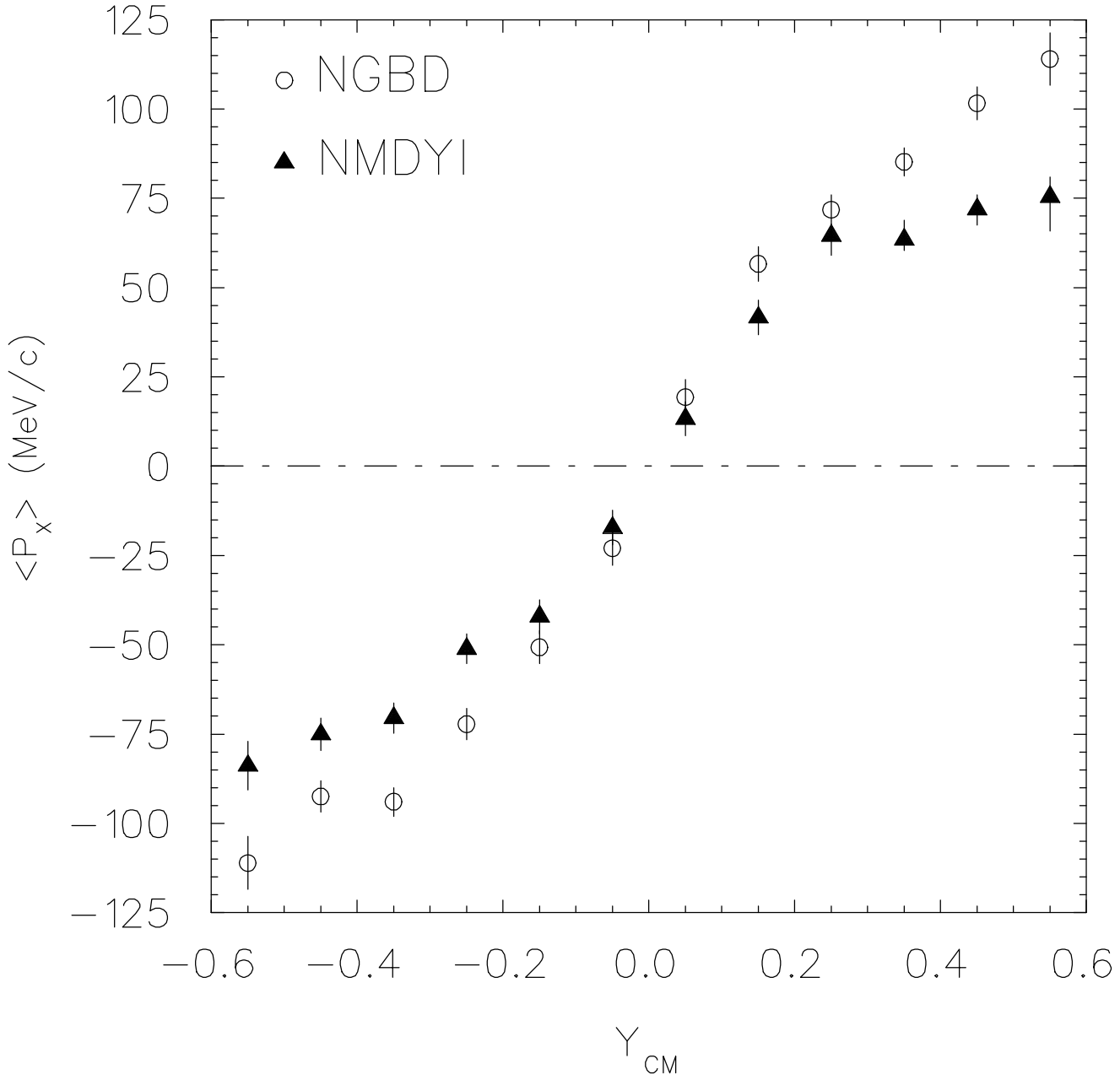
NGBD
NMDYI
125
100
75
50
25
0
−25
−50
−75
−100
−125
−0.6
−0.4
−0.2
0.0
0.2
0.4
0.6
<P_x> (MeV/c)
Y_CM

Fig. 5

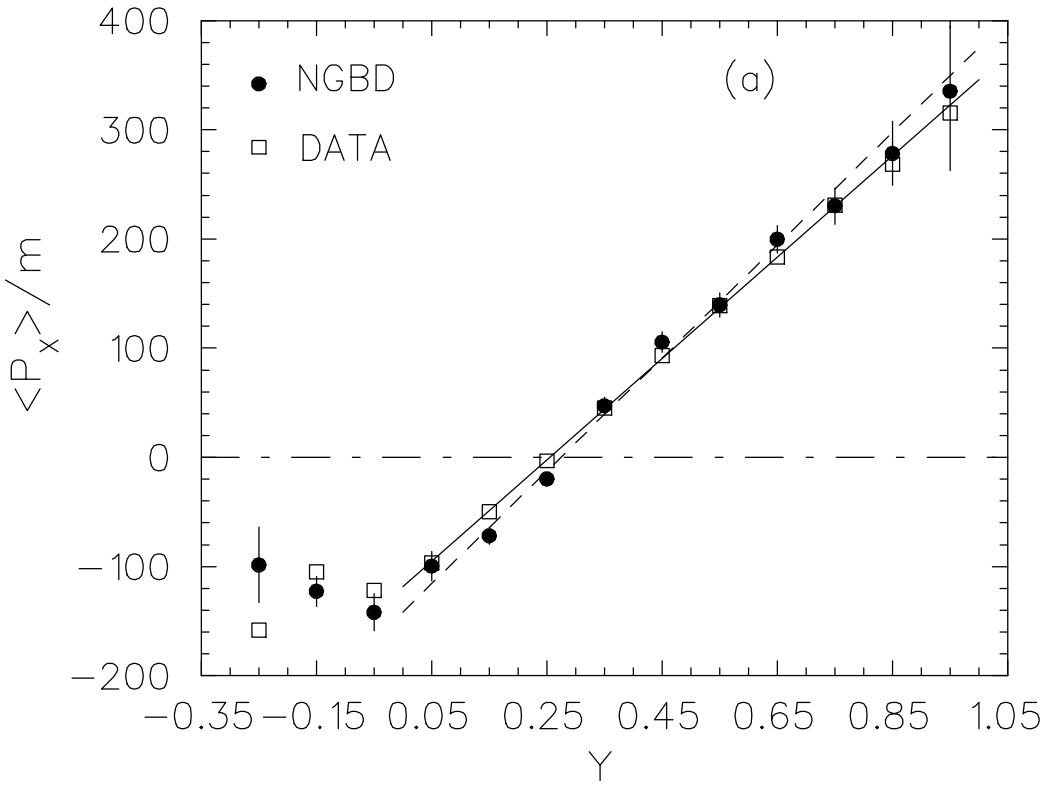
NGBD
DATA
(a)
<P_x>/m
Y
400
300
200
100
0
−100
−200
−0.35
−0.15
0.05
0.25
0.45
0.65
0.85
1.05

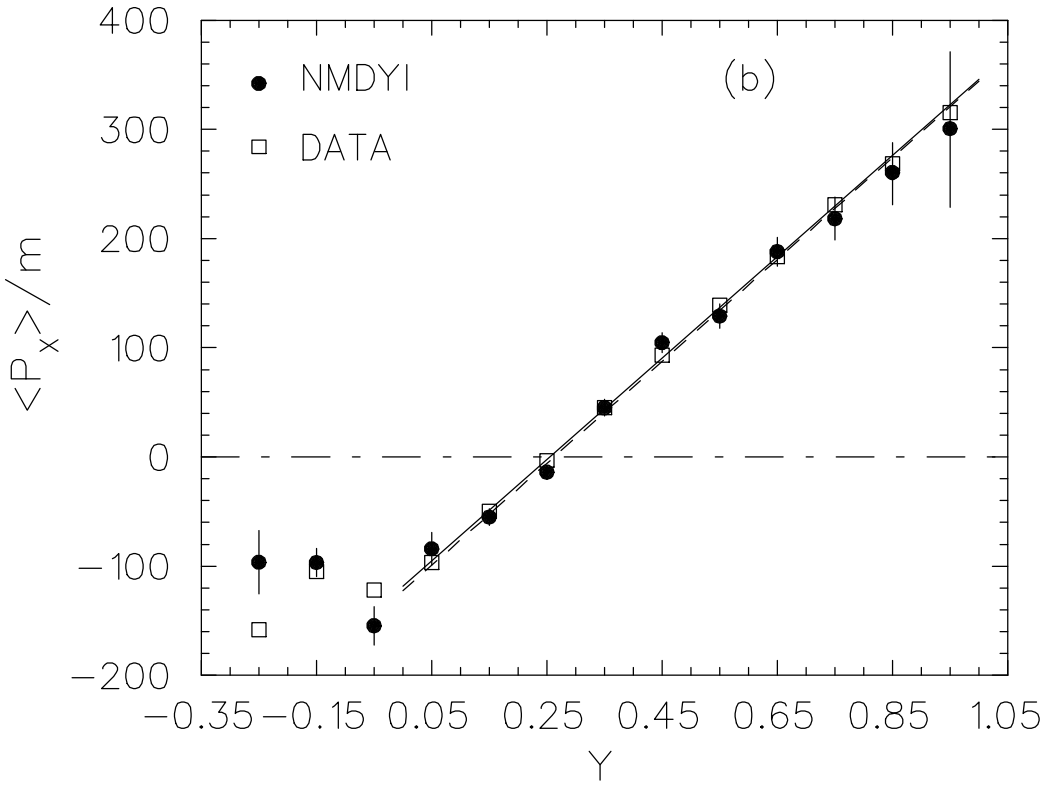
NMDYI
DATA
(b)
<P_x>/m
Y
400
300
200
100
0
−100
−200
−0.35
−0.15
0.05
0.25
0.45
0.65
0.85
1.05

Fig. 6

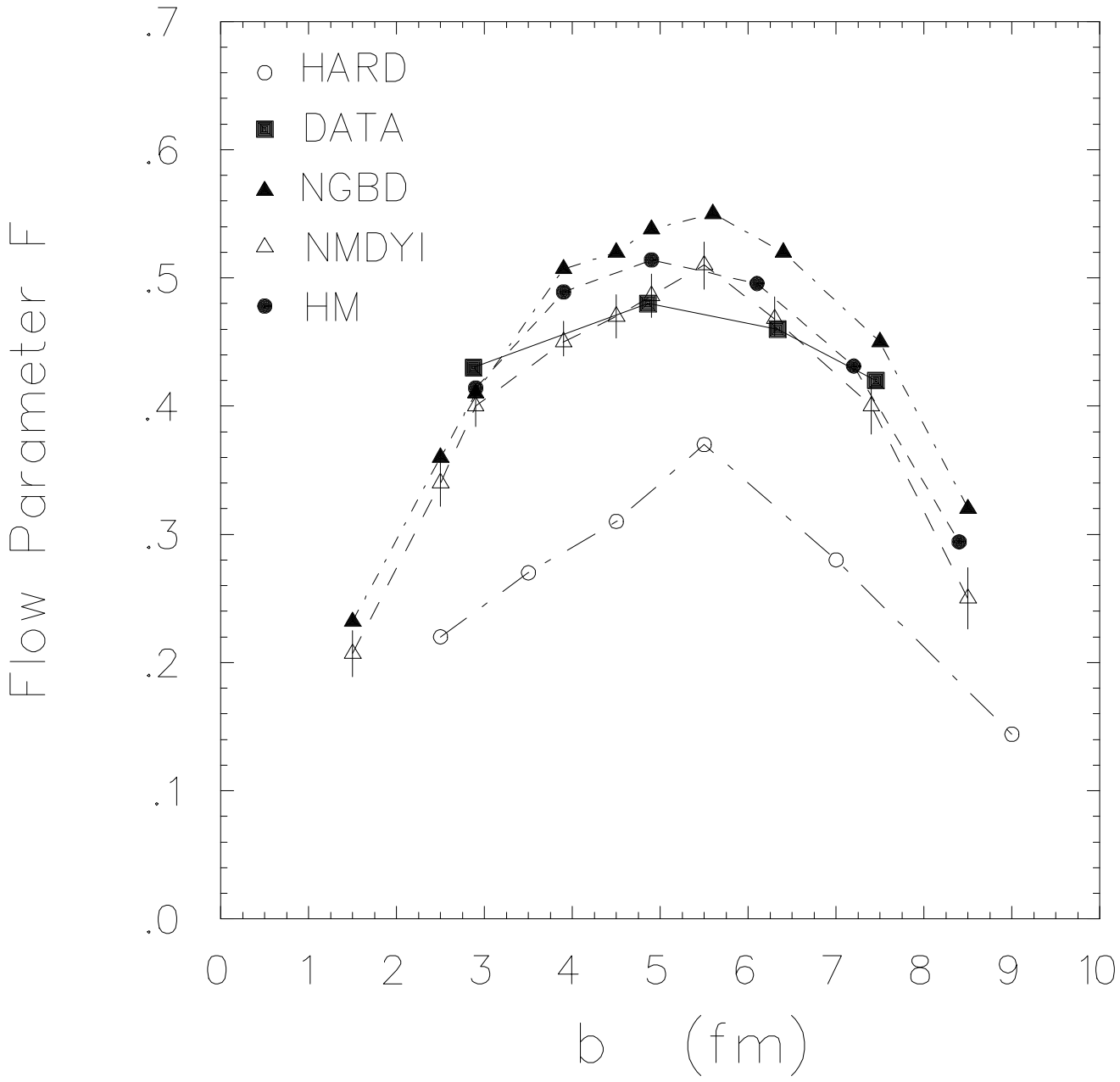
HARD
DATA
NGBD
NMDYI
HM
Flow Parameter F
.0
.1
.2
.3
.4
.5
.6
.7
0
1
2
3
4
5
6
7
8
9
10
b (fm)

Fig. 7

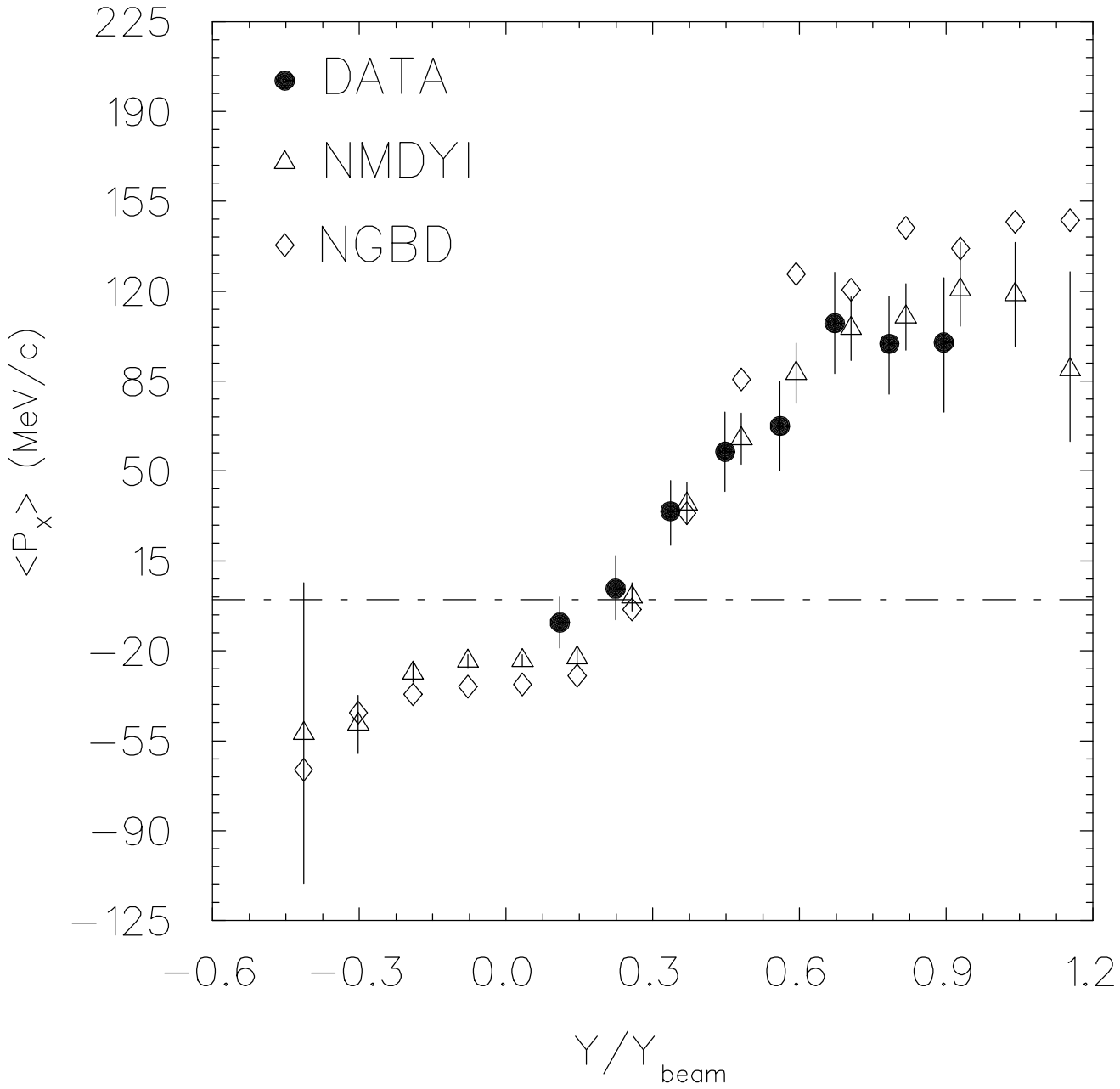
DATA
NMDYI
NGBD
225
190
155
120
85
50
15
−20
−55
−90
−125
−0.6
−0.3
0.0
0.3
0.6
0.9
1.2
<P_x> (MeV/c)
Y/Y_beam

Fig. 8

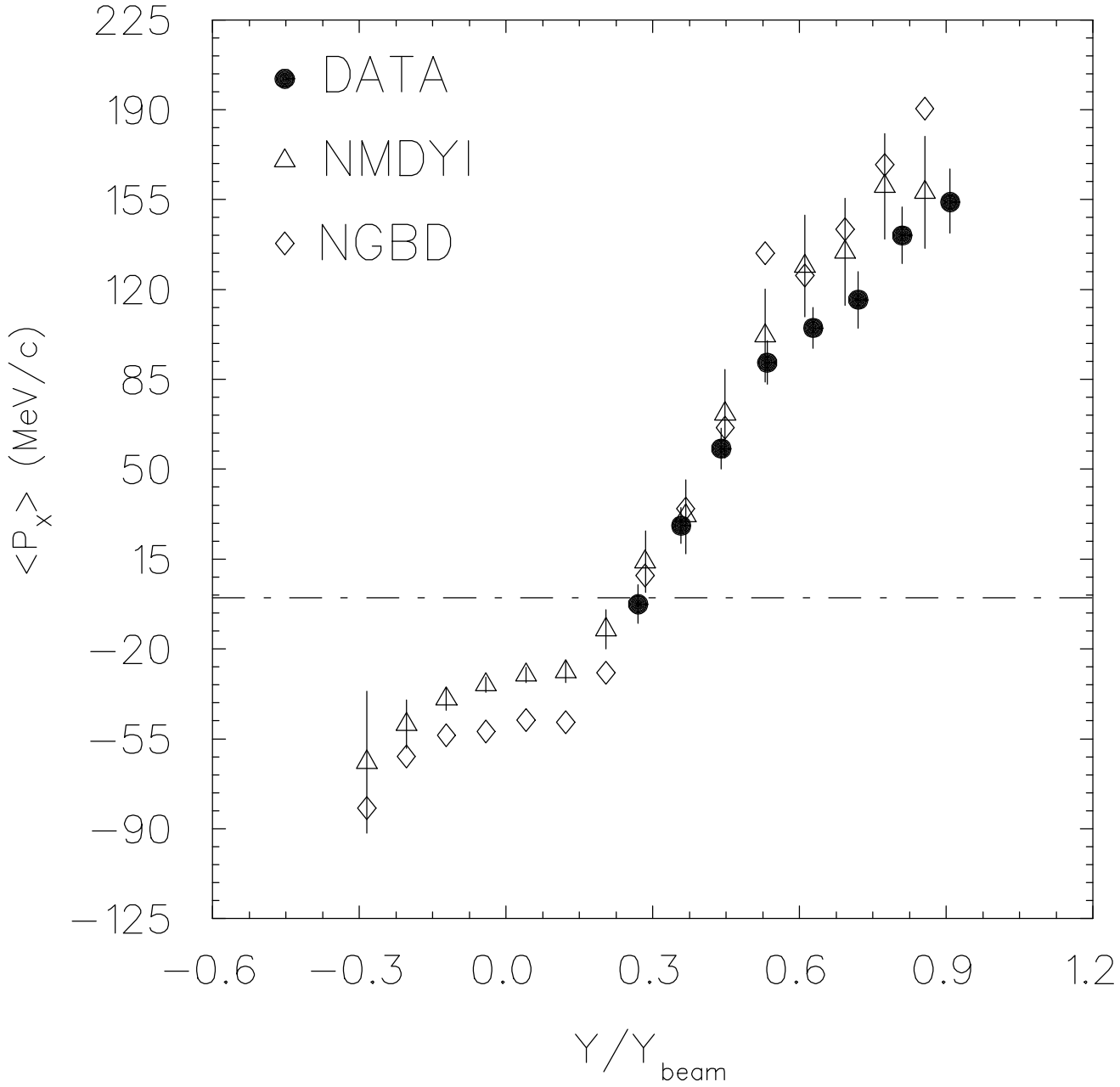
DATA
NMDYI
NGBD
225
190
155
120
85
50
15
−20
−55
−90
−125
−0.6
−0.3
0.0
0.3
0.6
0.9
1.2
<P_x> (MeV/c)
Y/Y_beam

Fig. 9

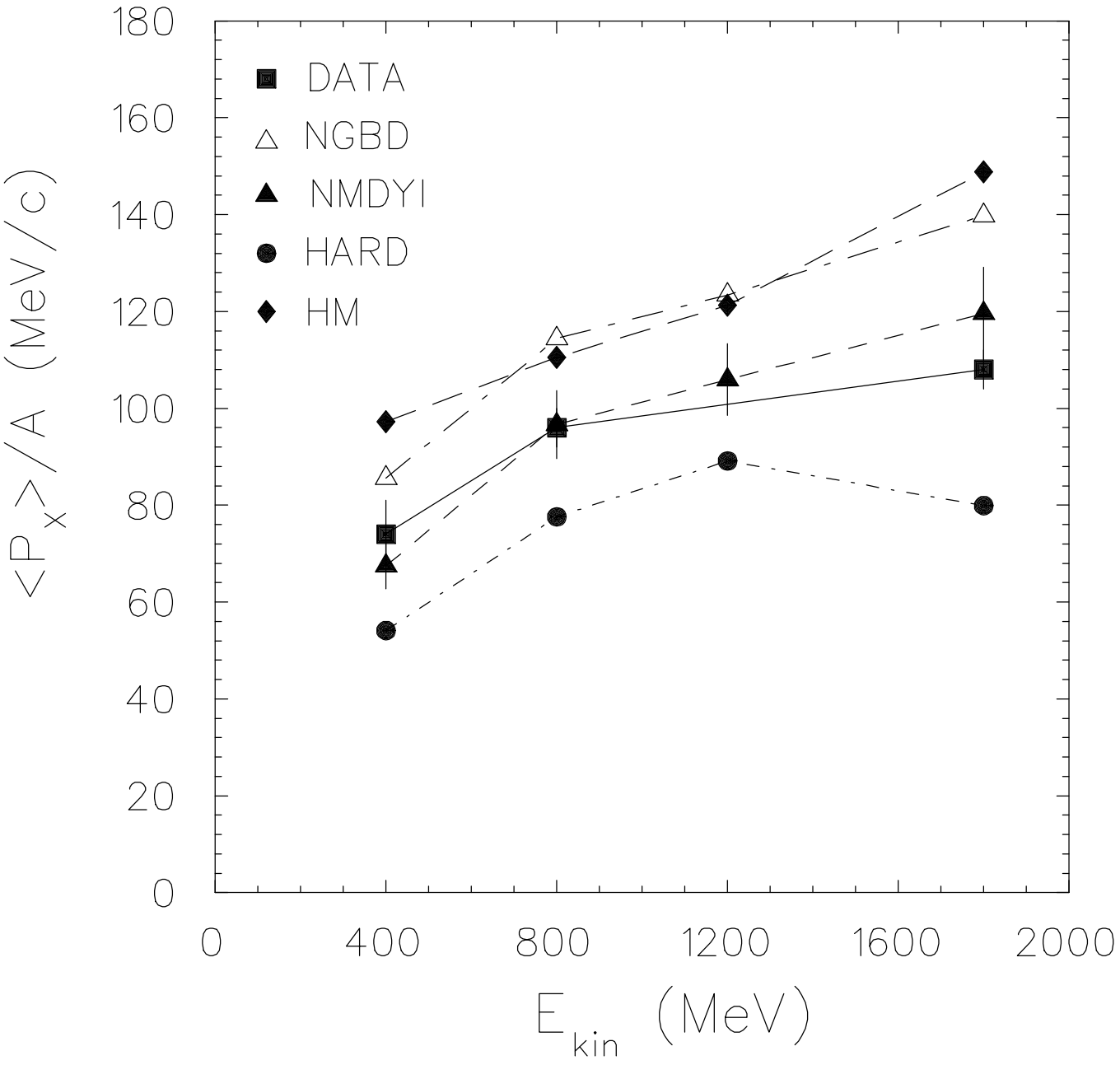
DATA
NGBD
NMDYI
HARD
HM
180
160
140
120
100
80
60
40
20
0
0
400
800
1200
1600
2000
$\langle P_x \rangle / A$ (MeV/c)
E_{kin} (MeV)

Fig. 10

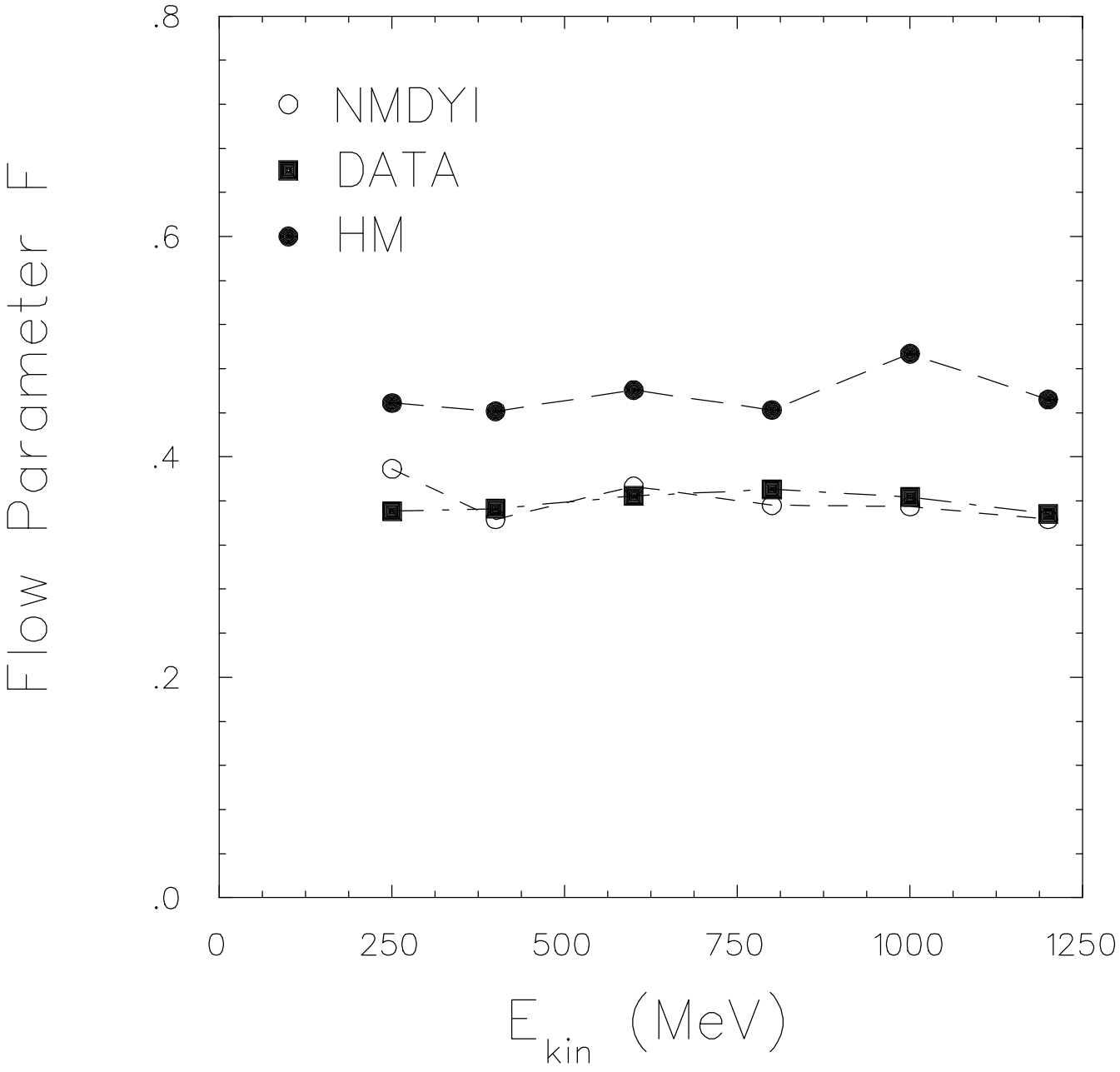
Flow Parameter F
.8
.6
.4
.2
.0
NMDYI
DATA
HM
0
250
500
750
1000
1250
E kin (MeV)

Fig. 11

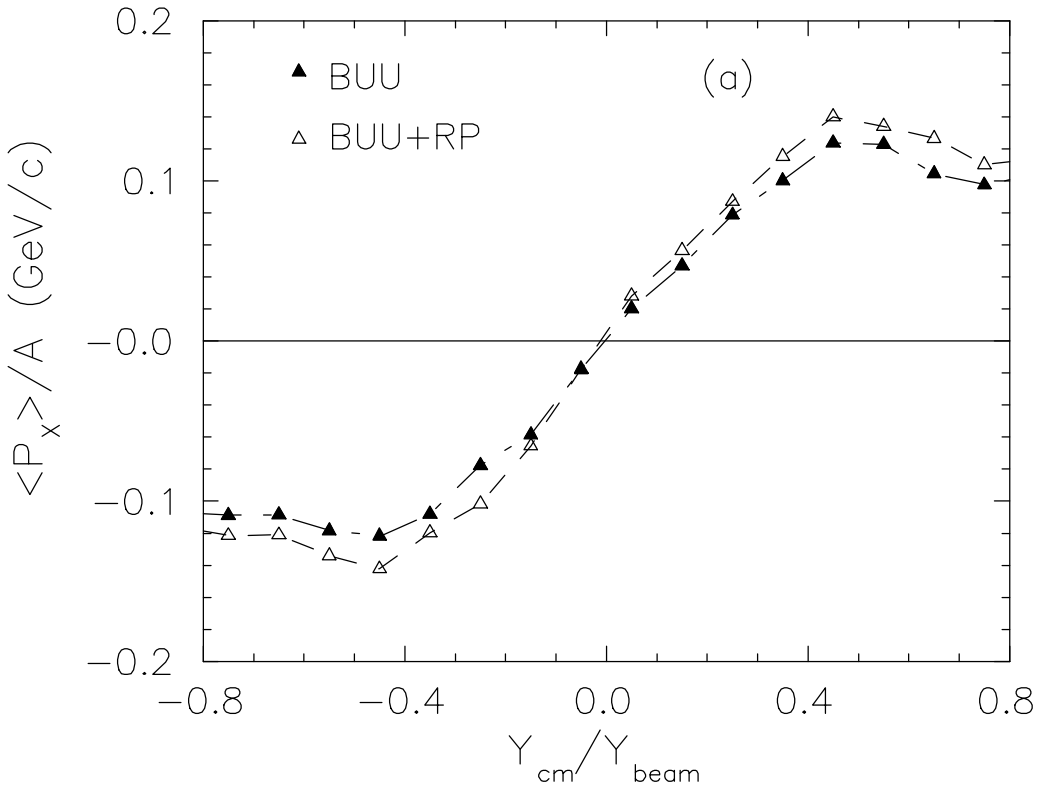
BUU
BUU+RP
(a)
<P_x>/A (GeV/c)
Y_cm/Y_beam
0.2
0.1
−0.0
−0.1
−0.2
−0.8
−0.4
0.0
0.4
0.8

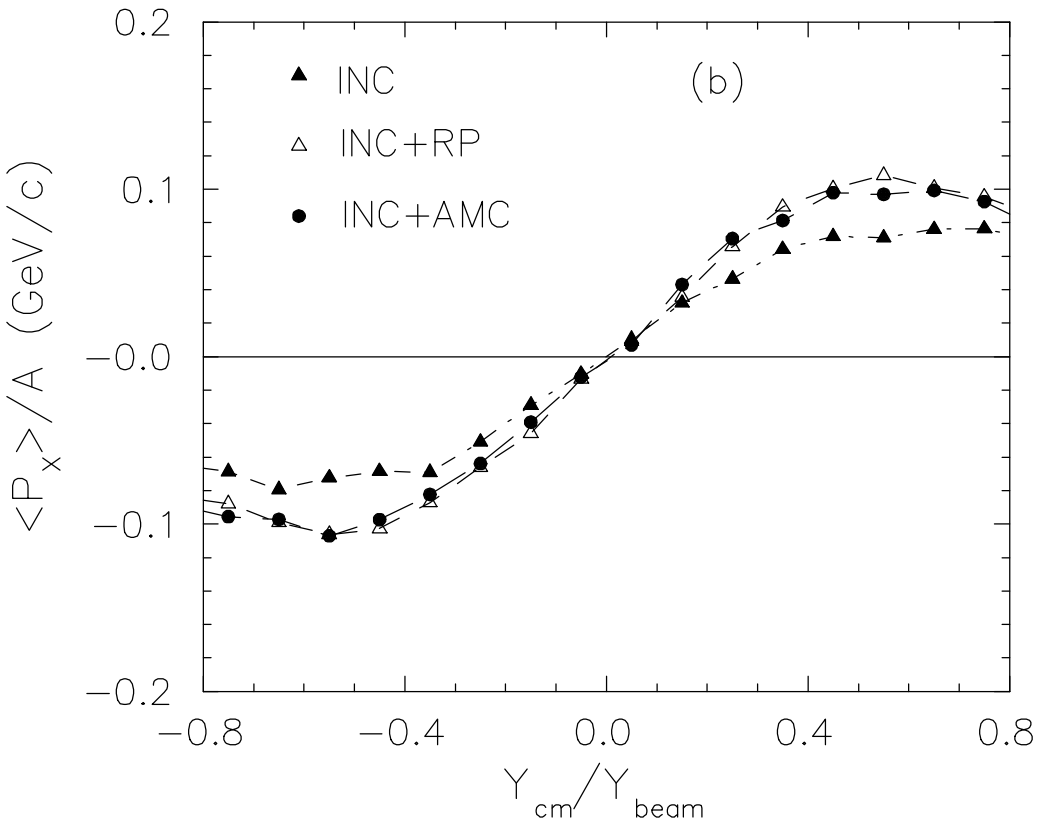
INC
INC+RP
INC+AMC
(b)
<P_x>/A (GeV/c)
Y_cm/Y_beam
0.2
0.1
−0.0
−0.1
−0.2
−0.8
−0.4
0.0
0.4
0.8

Fig. 12